HHS Public Access

Author manuscript

Annu Rev Anal Chem (Palo Alto Calif). Author manuscript; available in PMC 2022 July 27.

Published in final edited form as:

Annu Rev Anal Chem (Palo Alto Calif). ; 14(1): 299–321. doi:10.1146/annurev-anchem-091520-091009.

Protein Dynamics by Two-Dimensional Infrared Spectroscopy

Goran W. Tumbic, **Md Yeathad Hossan**, **Megan C. Thielges**

Department of Chemistry, Indiana University, Bloomington, Indiana 47401, USA

Abstract

Proteins function as ensembles of interconverting structures. The motions span from picosecond bond rotations to millisecond and longer subunit displacements. Characterization of functional dynamics on all spatial and temporal scales remains challenging experimentally. Two-dimensional infrared spectroscopy (2D IR) is maturing as a powerful approach for investigating proteins and their dynamics. We outline the advantages of IR spectroscopy, describe 2D IR and the information it provides, and introduce vibrational groups for protein analysis. We highlight example studies that illustrate the power and versatility of 2D IR for characterizing protein dynamics and conclude with a brief discussion of the outlook for biomolecular 2D IR.

Keywords

multidimensional; protein dynamics; 2D IR; infrared spectroscopy; vibrational probes; molecular recognition

INTRODUCTION

The protein structure-function paradigm continues to evolve. Our understanding of protein biophysics has progressed from static structures to interconverting ensembles of conformational states represented by a hierarchical energy landscape (1–3). Protein motions range from local bond rotations to global subunit displacements that span a wide range of timescales, from picoseconds to seconds and longer. Specific regions of a protein may varyingly contribute to function. Larger-scale backbone motions are clearly central to (mis)folding and allosteric regulation, while side chains are the parts of proteins subject to evolution that ultimately tailors protein biophysics. Characterization of all the potentially important motions, however, remains experimentally challenging. Two-dimensional infrared spectroscopy (2D IR) is emerging as a powerful approach to investigate protein dynamics owing to its inherently fast timescale, structural sensitivity, and capability for site selectivity. 2D IR has enlightened diverse aspects of protein biophysics, ranging from protein folding to enzyme specificity (4–8).

Here, we present an overview of advances in 2D IR directed at elucidating protein structural dynamics. We point out the advantages of IR spectroscopy generally, introduce the basics of the 2D IR experimental approach and information content, then consider the vibrations used

thielges@iu.edu .

The *Annual Review of Analytical Chemistry* is online at anchem.annualreviews.org

as probes of proteins. We illustrate the utility and diversity of 2D IR applied for investigating proteins and their dynamics through a brief presentation of select examples. Finally, we discuss the next directions for advancing the methods and expanding the scope of protein 2D IR.

ADVANTAGES OF INFRARED SPECTROSCOPY FOR STUDY OF PROTEIN DYNAMICS

IR spectroscopy is well suited for measuring protein states and dynamics owing to its inherently fast timescale. The feasibility to capture two states depends on the difference in the frequencies of the spectroscopic markers and the timescale of their interconversion. Fast interconversion can lead to averaging of signals and masking of information about populated states. The relatively high-energy scale of IR spectroscopy enables capture of states interconverting as rapidly as picoseconds. Most protein motions are slower and appear static on the picosecond timescale. Thus, an IR spectrum provides a snapshot of the ensemble of populations. In addition, ultrashort IR pulses can be generated to follow processes in real time with high temporal detail.

Another advantage of IR spectroscopy is the spatial resolution. Some vibrations are as small as a bond and local mode in character. Their absorptions can probe specific local sites in proteins and tackle the challenge of the complex spatial heterogeneity (9). Other vibrations of proteins involve many atoms and provide more global information. For example, analysis of delocalized amide backbone vibrations informs about global protein secondary structure (4, 5, 8, 10). Although IR spectroscopy has the potential to capture local and global protein vibrations, spectral congestion can make detection and assignment of specific absorptions unfeasible in practice. The richer information afforded by 2D methods helps to alleviate this challenge.

FUNDAMENTALS OF TWO-DIMENSIONAL INFRARED SPECTROSCOPY

The theory and methods of 2D IR have been presented extensively (11–14); here, we limit discussion to a basic description required to understand how 2D IR informs on protein dynamics. 2D spectra report connections among transitions along two frequency axes (Figure 1). One axis demarks the frequencies pumped or excited at an initial time. The second axis demarks frequencies probed or detected at the same or later time. The time interval between pumping and probing is typically referred to as the waiting time, T_w. Consider the simplest 2D spectrum of a single vibrational transition (Figure 1a). The 2D spectrum contains a pair of bands. A band at the fundamental (0–1) frequency appears along the diagonal, and a band of opposite sign appears at the 0–1 frequency along the pump axis and at excited state absorption frequency (1–2) along the probe axis. The diagonal and off-diagonal bands reflect that pumping at the 0–1 frequency results, respectively, in probing a ground state bleach and stimulated emission at the 0–1 frequency and excited state absorption at the 1–2 frequency. The unacquainted should note that varying plotting conventions are used for the pump and probe axes and the absolute signs of the bands. When multiple species are present, multiple 0–1 bands appear along the diagonal. Off-

diagonal intensity indicates that the transitions at the pump/probe frequencies are connected, providing direct evidence that the species either interconvert or are in some way coupled.

2D spectral data are acquired either in the frequency domain directly or in the time domain, followed by Fourier transform to a spectrum (12). The most prevalent implementation of the experiment obtains the pump spectral data in time and the probe data in frequency. A series of three, ultrashort IR pulses are applied to interact with a sample (Figure 1a). The evolution between the first and second pulse effectively labels the system with the initial frequencies in the sample ensemble; Fourier transformation along this time evolution generates the pump frequency axis. After a delay of T_w, the third pulse is applied, and the sample emits a third-order signal in the direction of the wave vector sum of the three excitation pulses. The signal must be heterodyne-detected by overlap with a local oscillator, either a fourth pulse or the probe beam itself, to obtain phase information necessary for generation of the pump spectrum. The overlapped signal/local oscillator is passed through a spectrograph to instrumentally perform the Fourier transform and generate the probe frequency axis.

2D IR instrumentation and methodology have developed over the past two decades (10, 15–23). Temporal control of pulse timing may be performed with conventional mechanical delay stages or through pulse shaping. The conventional approach typically is implemented in a non-collinear beam geometry that results in emission of the third-order signal into a unique direction. Background-free detection affords higher sensitivity, but data acquisition is slower. In contrast, pulse shaping typically is implemented in a pump-probe beam geometry that results in emission of the third-order signal colinear with the probe beam. This approach allows for rapid data collection and simplifies spectral processing, but to the detriment of sensitivity. Many of the drawbacks of both approaches can be alleviated or eliminated by further tailoring the instruments and methods (24–28). These and other variations in 2D IR methodology provide versatility for adapting to the distinct technical challenges in investigating diverse questions and samples.

ADVANTAGES OF TWO-DIMENSIONAL METHODS

Deconvolution of Absorption Bands

Proteins have many vibrational modes and usually many instances of the same bond types. Thus, spectra contain many bands that absorb at similar frequencies. An individual oscillator also may experience multiple environments associated with protein states, resulting in multiple absorptions. Moreover, IR spectroscopy captures essentially all the microstates owing to the rapid inherent timescale. Each of the protein or solvent configurations surrounding an oscillator causes variation in frequency. As a result, bands often show substantial inhomogeneous broadening. The spectral congestion from the superposition of many, overlapping, broad absorption bands can make detection and assignment of a single vibration within a protein unfeasible in practice. 2D IR has distinct features that can facilitate spectral deconvolution.

A useful difference between 1D and 2D absorptions is the dependence on transition dipole (TD) strength of the vibration (12). Band intensity in 2D spectra scales as the fourth power of the TD strength, while in 1D spectra it scales as the square; thus,

the 2D bands are squared relative to the 1D. This effectively narrows each band in the 2D spectrum, enhancing spectral resolution. In addition, vibrations of interest for characterization of protein dynamics often have larger TD strength than those of aqueous solvent, so their absorptions are enhanced above the background. These features are particularly advantageous for analysis of amide backbone vibrations. As an example, the 2D spectrum, 2D diagonal spectrum, and 1D spectrum for the amide region of α-synuclein are shown in Figure 1b (29). The 2D data accentuate a band at ~ 1,620 cm^{-1} associated with strong TD coupling among amides in β-sheet structure.

The difference in dependence of 1D and 2D absorptions on TD strength also enables better quantification of populations of associated protein states (30, 31). Obtaining a calibration curve to rigorously determine the spectral response for individual states of a protein is not usually possible. However, the ratio of the 2D and squared 1D absorptions provides their relative TD strengths and thereby enables more accurate quantification of the relative populations. To illustrate, the 1D spectrum of carbon monoxide (CO) ligated to the cytochrome P450cam-putidaredoxin complex shows a shoulder at high frequency that is accentuated in the 2D spectrum due to larger TD strength (Figure 2a) (32). The relative areas of the 2D and 1D bands indicate that the high-frequency component has ~1.3-fold larger TD strength. This knowledge enables accurate quantification of the two populations of the protein.

Another feature of 2D IR that can assist deconvolution of superimposed bands is the T_w dependence of the 2D band intensity. The intensity decays with the excited state lifetime of a vibration (12, 33). Thus, if vibrations of multiple species have different lifetimes, the intensity of each band will decay distinctly with T_w. This T_w dependence can be harnessed to uncover overlapping component bands. For example, T_w-dependent 2D spectra of CO ligated to the cytochrome P450cam-putidaredoxin complex that contain two unresolved bands are shown in Figure 2b (32). Because the vibrational lifetime for the low-frequency band is shorter, the band decays more rapidly, and 2D spectra taken with sufficiently long T_w can isolate the high-frequency component.

Deconvolution of Line Broadening

IR spectroscopy captures essentially all the vast number of potential microstates experienced by a vibration in a protein or aqueous environment, which leads to substantial inhomogeneous broadening. Conversely, the inhomogeneous line width of an absorption provides a measure of heterogeneity. However, line broadening also has homogeneous contributions from the finite excited state lifetime, orientational dynamics, and dynamics that are fast on the IR timescale (i.e., $\Delta\nu\Delta\tau < 1$, where $\Delta\nu$ is the frequency deviation and $\Delta\tau$ the timescale of interconversion). The contributions to line broadening are convoluted in 1D spectra and cannot be rigorously extracted. 2D IR informs about broadening mechanisms through the 2D lineshapes (12, 34, 35). The distribution of states that underlie inhomogeneous broadening is static on the IR timescale, so when 2D spectra are taken with a T_w of zero, the ensemble has the same pump and probe frequencies and contributes to intensity along the diagonal. As a result, the elongation of the 2D band along the diagonal provides a measure of the inhomogeneous broadening (Figure 2b).

Dynamics Among States: Conformational Exchange and Spectral Diffusion

T_w-dependent 2D IR enables direct measurement of the dynamics of interconversion among states (36). In a simple case of two populated states, two bands at the fundamental frequencies will appear along the diagonal of a 2D spectrum taken with a T_w of zero (Figure 2d). As T_w is lengthened, if states interconvert between pumping and probing, crossbands will grow in at the corresponding frequencies. Analysis of the time dependence of the crossband areas provides the timescale of exchange dynamics. For example, T_w-dependent 2D IR of CO-ligated myoglobin has enabled quantification of exchange rates between two side chain rotamers (36).

Analogously, the dynamics among an inhomogeneous distribution of states can be determined from T_w-dependent 2D spectra, but the dynamics are manifest by changing band shape (32, 37–40) (Figure 2b). When T_w is short, the inhomogeneous distribution causes the 2D spectra to appear highly elongated along the diagonal because most of the ensemble has the same pump and probe frequencies. As T_w is lengthened, the states have increasing time to interconvert between pumping and probing, leading to growth in off-diagonal intensity. This causes the 2D band shape to become less diagonally elongated as the underlying states interconvert.

Several analytical methods are in use for quantifying the band shapes. A widely applied one is center-line-slope (CLS) analysis (34, 35). An alternative is band ellipticity (40). Another metric, preferable if the 0–1 and 1–2 bands of opposite sign overlap, is the nodal slope between the bands (38, 41). Regardless of method, the key utility is that the time dependence reflects the dynamics among the frequency inhomogeneity (Figure 2c). Combining information about the 2D band shape dynamics and the 1D spectrum, a frequency-frequency correlation function can be obtained that fully quantifies the line broadening and dynamics (34, 35, 42). Examples of this approach to quantify dynamics at side chains of calmodulin (CaM) and cytochrome P450 are described in later sections.

Vibrational Coupling

When vibrational modes interact, whether through electrostatic, dipole, or mechanical mechanisms, they become energetically coupled. Coupling leads to shifts in the uncoupled band frequencies. 2D spectra furthermore provide unambiguous evidence for coupling by the presence of crossbands at the frequencies of the coupled modes (10, 43) (Figure 1c). Accentuation of the crossbands is possible using cross-polarized excitation pulses (43, 44). Their intensity reflects the strength of the coupling between modes. Because the strength of through-space coupling depends on the proximity and relative orientation of the coupled modes, the crossbands are highly sensitive to molecular structure and intermolecular interactions. Therefore, they are useful for assigning and interpreting complex IR spectra and evaluating structural models. Analysis of crossbands due to TD coupling between amide modes has been applied extensively to characterize secondary structure (4, 5, 8, 10). TD coupling between side chain vibrations has been detected within a trimer peptide, demonstrating potential in the future for monitoring tertiary structural changes of proteins (45).

VIBRATIONAL PROBES OF PROTEINS

2D IR may be directed at the amide backbone, side chains, or ligands. The diversity of probes provides versatility for characterizing protein dynamics at their varying spatial levels, from global subunit displacements to side chain wiggling. Besides the investigated protein and question, a practical consideration for selection of probe vibration is whether or how rigorously the absorptions can be detected and interpreted. The achievable concentrations of protein solutions are limited, so vibrations with intense absorptions are desirable. Spectral selectivity is a major concern because of spectral congestion, complicating the characterization of specific parts of proteins. Moreover, some vibrational modes are local in character, so they provide information about specific locations. Others are delocalized and inform about larger-scale structure. For detailed discussion of vibrational probes employed for 1D or 2D IR, we guide readers to comprehensive reviews (8, 9, 33). Theoretical efforts to assist interpretation have developed in parallel with experimentation (14). Below, we briefly introduce the vibrational groups that have been employed to study proteins by 2D IR.

Ligands

Many ligands have vibrations at frequencies in a spectral region free of native protein absorptions (1,800–2,300 cm^{-1}) useful for characterizing environments within proteins. Some of the first demonstrations of 2D IR were directed at a CO ligand of the hemeprotein myoglobin (46, 47) (Figure 2c). Many 2D studies have utilized CO and other small-molecule ligands owing to their intense, spectrally resolved absorptions (48–53). Inhibitors and transition-state analogs have enabled the study of enzyme active sites (54–57). An advantage of ligands is that the local environment probed is usually functionally critical. Ligands, however, are limited in application to the one or select proteins that bind them and for characterization of the location where they bind.

Amide Vibrations

2D IR of the amide vibrations of a protein backbone is well developed (4, 5, 8, 10). The amide I mode, described roughly by the carbonyl stretch, is the most commonly analyzed vibration. Strong TD coupling among amide I vibrations leads to delocalized vibrations that absorb at frequencies characteristic of particular secondary structures (Figure 1c). The TD strength of the delocalized vibrations increases with the number of coupled oscillators, thus quantifying the extent of the secondary structure. Moreover, crossbands in 2D spectra between coupled amide vibrations strongly substantiate the presence of a particular structure (4, 43, 58–63) (Figure 1b,c). Because the intensities of the crossbands reflect the strength of the coupling, which depends on the separation and orientation of the TDs, the 2D crossband data provide experimental constraints for modeling protein structure (10, 64–67).

Bands in the amide frequency region are diagnostic of protein within a biological sample but generally not selective within a protein. However, in some cases, dynamics of particular regions of proteins can be isolated by difference spectroscopy (4, 63, 68, 69). Another approach to achieve selectivity is $^{13}C^{18}O$ labeling of the amide backbone at specific residues (61, 65, 67, 70–73). Isotopic labeling downshifts absorptions into a spectral region with less congestion. The region also contains absorptions of acidic side chain

vibrations, but the $^{13}C^{18}O$ absorption can be isolated by subtraction with unlabeled samples. The frequency disparity between labeled and natural abundance amides also disrupts TD coupling. This can assist spectral interpretation by distinguishing features due to coupling from hydrogen bonding, local electrostatics, and other mechanisms. For example, a newer method, dihedral indexing, compares crossbands for samples isotopically labeled at two residues simultaneously and individually to verify and better measure their coupling (74). $^{13}C^{18}O$ incorporation at specific residues in peptides is straightforward via solid-phase synthesis, and labeling of larger proteins can be achieved by ligation of peptides to larger protein fragments. 2D IR of the ion channel KcsA selectively labeled by semisynthesis is presented in a later section.

Native Side Chain Vibrations

Although the spectral regions of native side chain absorptions are generally congested for even small proteins, in some cases, characterization of native vibrations of side chains is possible by 2D IR. Difference spectroscopy can isolate absorptions of individual or a few side chains. For example, 2D IR has probed carboxylate side chains (69), and isotopic labeling can improve spectral resolution (75). Sulfhydryl groups of cysteine residues have been detected in hemoglobin by 2D IR (76). For this group, spectral congestion is not an issue, but the absorptions are very weak. Several additional native side chain vibrations have potential as 2D IR probes of proteins. The ring breathing mode of tyrosine has been detected in a Trp cage miniprotein (77). Vibrations of the guanidyl group of arginine are sensitive to salt bridge interactions, which often play key roles in protein tertiary and quaternary structure (78, 79).

Nonnative Side Chain Vibrations

An approach to achieve spectral selectivity is to introduce noncanonical amino acids with vibrational groups that absorb in the transparent frequency window of protein spectra (9, 33). A variety of noncanonical amino acids functionalized with cyano, azido, or metal carbonyl groups with spectrally resolved vibrations have been employed for protein 2D IR (22, 80–93). Such groups can be introduced as vibrational probes in principle at any location. Although their utilization for 2D IR remains much more limited than for 1D spectroscopy, detection of single vibrations in proteins is possible. A handful of studies have demonstrated their potential for characterizing multiple sites to comprehensively analyze protein structure and dynamics (87, 90–93).

In addition to strong, distinguishable signals, vibrational lifetime is a property of the probe important for 2D IR of dynamics. The intensity of 2D signals decays with vibrational relaxation, so the lifetime determines the experimental time window. In general, the TD strengths of probes are stronger when attached to aryl than alkyl side chains, whereas the vibrational lifetimes are typically longer for alkyl than aryl probes (9, 33). Smaller probe groups attached to side chains isostructural with the native residues are preferable to minimize functional perturbation. There also are practical considerations when introducing particular nonnative amino acids at specific locations in proteins (9). Direct incorporation via synthesis is limited to peptides or small proteins (94–98); semisynthesis is possible (99–101), but involved, and has not yet been utilized for 2D IR studies of side chains. Specific

incorporation by chemical modification of native side chains or auxotrophic expression requires that the labeled side chain be unique within a protein (22, 87, 89, 92, 102). Labeling by amber suppression, via expression systems evolved for the particular noncanonical amino acid, can access larger proteins without introducing additional modifications, but studies have been currently limited to aromatic amino acids (80, 90, 91, 103). Labeling by cell-free synthesis is possible but not yet employed for protein 2D IR (104).

Azido groups are attractive as 2D IR probes owing to their large TD strengths (80, 83, 87–89). Indeed, their strong signals have made possible detection of 2D spectra of single probes in protein samples at concentrations as low as 100 μM (88). Studies have utilized azido probes at aryl and alkyl side chains of proteins through selective incorporation of azidophenylalanine by amber suppression and azidohomoalanine by expression in methionine auxotrophic bacteria, respectively (80, 89). A disadvantage of azido groups is that their vibrational lifetimes are typically short, and they are relatively large with greater potential for perturbation. Fermi resonances can also complicate interpretation (105).

In comparison, cyano groups are smaller but have weaker absorptions. Analysis by 2D IR currently requires protein samples at minimal ~1 mM concentration (22, 90–92). However, their longer vibrational lifetimes facilitate measurement of spectral dynamics. Cyanophenylalanine (*CN*F) serves as a reasonable analog for phenylalanine or tyrosine, provides moderately strong signals, and may be incorporated into larger proteins via amber suppression methodology (90, 91, 93, 95–97). Thiocyanate (*CN*S) can be introduced in proteins via cyanylation of unique cysteine residues (22, 92). While the absorptions are much weaker than those of *CN*F, their approximately 10–20-fold longer lifetime greatly extends the experimental time window (106). The cyano group of cyanotryptophan provides strong signals that are promising as 2D IR probes of proteins (45).

Metal carbonyl complexes can be attached via side chains to the surface of proteins (81, 82, 84–86). They provide intense 2D IR signals that permit study of samples at lower protein concentrations. While the large size limits their incorporation at the protein exterior, they provide useful probes of surface electrostatics and hydration dynamics.

APPLICATIONS

Amide Backbone Dynamics

2D IR studies directed at amide vibrations follow the backbone structure and interactions of proteins. Amide 2D IR has been utilized by a substantial body of research to investigate protein folding and aggregation (4, 8).

Folding.—Studies of folding dynamics are fundamentally important to understanding the potential energy landscape of proteins, as well as the origins of (mis)folding. 2D IR has examined equilibrium unfolding by thermal and chemical denaturation (107–109). Measurement of kinetics requires addressing the additional technical challenge of rapidly triggering a reaction. 2D studies have implemented laser-induced temperature jump and photo-triggering for initiating peptide or protein unfolding (63, 72, 110–116). 2D spectral snapshots then monitor protein structural changes over time.

As an example, we present transient 2D IR combined with temperature jump to uncover mechanistic details of insulin dimer dissociation (63). Shown in Figure 3 are 2D IR difference spectra from equilibrium collected at varying times after rapidly heating by vibrational excitation of water with a nanosecond laser pulse. The difference spectra taken with cross-polarized pulses accentuate the crossbands. These spectra show crossband patterns characteristic of the loss of β-sheet structure 320 μs after triggering unfolding. Later, at 560 μs, the difference spectrum taken with parallel pulses shows a spectral pattern that arises from a diagonal band shift. This shift reports on dimer dissociation. The study demonstrates how 2D IR features can clearly dissect kinetic folding mechanisms, in this example revealing local unraveling of secondary structure prior to dimer dissociation.

Aggregation.—Amyloid formation has been implicated in numerous diseases and disorders, ranging from neurodegenerative diseases, such as Parkinson's and Alzheimer's diseases, to diabetes and cataracts (117). The structural sensitivity of 2D IR, combined with advances in rapid data collection, have been leveraged to gain molecular-level insight into the process of peptide aggregation and amyloid fibril formation under a variety of conditions (118–124). 2D IR has uncovered critical but elusive oligomeric intermediates during the formation of larger aggregates and contributed to elucidating the origins of different fibril morphology (29, 123–128). Integrated studies of aggregation are combining 2D IR with more conventional techniques for fibril analysis to connect molecular and larger-scale information (121, 123, 125, 129).

As an example of how 2D IR provides molecular details about aggregation, we point to a study directed at human islet polypeptide (hIAPP), a polypeptide present in amyloid plaques associated with type 2 diabetes (61). 2D spectra taken during aggregation of hIAPP selectively labeled with $^{13}C^{18}O$ provide a residue-specific view of a reaction intermediate (Figure 4). The natural abundance amide absorptions report a sigmoidal transition from frequencies characteristic of a global transition from random coil (~1,645 cm^{-1}) to parallel β-sheet structure (~ 1,620 cm^{-1}) (Figure 4b). Absorptions associated with β-sheet structure at the individual isotopically labeled residues can be observed at downshifted frequencies (Figure 4c, *red arrows*). For V17 and G33, the downshifted isotope absorptions follow the global transition from random coil to β-sheet structure. In contrast, for residues F23, G24, A25, and L27, the downshifted absorptions appear early during the lag phase, then disappear. These absorptions provide evidence that these residues temporarily participate in a β-sheet intermediate, before finally adopting loop structure. The study illustrates how 2D IR spectroscopy in combination with selective labeling can afford residue-specific views of kinetic reaction intermediates in amyloid formation.

Molecular Recognition

Protein molecular recognition underlies cellular function. Protein dynamics fundamentally affect affinity through entropic contributions to free energy, modulate specificity of binding partners or catalysis on a substrate, and underlie allostery that communicates binding events through proteins. Studies by 2D IR have afforded insight into the molecular recognition of ions, small molecules, peptides and proteins, and were directed at ligands, the backbone, native side chains, and nonnative side chain probes (67, 69, 92, 93). Below, we present select

examples to exhibit the diverse applications, highlighting the information available by 2D IR.

Ion channel permeation.—The mechanism of selective ion transport, such as through ion channels that underlie action potentials in excitable cells, has been under longstanding investigation (130). The ion channel KcsA mediates K^+ ion transport across membranes through coordination by a series of backbone carbonyl groups (Figure 5a). Two models have been proposed for ion permeation: the knock-on model in which ions are separated by water molecules and the hard-knock model that proposes ion–ion collisions without intervening water (131, 132). Application of 2D IR with selective $^{13}C^{18}O$ amide labeling is able to differentiate these models (67).

The 2D spectrum acquired of KcsA labeled with $^{13}C^{18}O$ at three of the residues of the selectivity channel is shown in Figure 5b. Isotope labeling downshifts the vibrational frequencies to a less-congested frequency region, and subtraction with the spectrum of unlabeled KcsA isolates the $^{13}C^{18}O$ amide absorptions. The presence of a set of bands in the spectrum indicates two distinct environments or states of the labeled residues. Comparison of this spectrum and those calculated based on the TD coupling in structural models of the selectivity channel provides clear support for the knock-on mechanism.

Furthermore, the simulated spectrum best matches the experimental one when generated with contributions from populations of three channel configurations (Figure 5c). Interestingly, for 40% of the population, the backbone of one residue (V76) flips outward from the pore. The states are observed in molecular dynamics simulations, but the small differences among their energies prevent reliable determination of populations. This work demonstrates direct experimental quantification of such rapidly interconverting states via 2D IR, highlighting the advantage of its fast timescale.

Distinct recognition of Ca^{2+} ions by calmodulin.—CaM is a ubiquitous intracellular Ca^{2+} sensor (133). Ca^{2+} binding to CaM induces conformational changes that capacitate recognition and activation of a wide range of effector proteins that orchestrate cellular communication. Cellular assays of CaM function often employ lanthanide ions, e.g., lanthanium (La^{3+}), in replacement of Ca^{2+} to take advantage of their luminescent properties. However, comparison by 2D IR reveals subtle differences in the ions' recognition by CaM (69).

2D spectra collected for the apoprotein, Ca^{2+}-bound, and La^{3+}-bound states of CaM with two T_w and their difference are shown in Figure 6a. The 2D spectra for Ca^{2+}-bound CaM uniquely show a band at 1,550 cm^{-1} characteristic of a carboxylate with bidentate ion coordination. This feature is assigned to bidentate coordination of Ca^{2+} by a conserved glutamic acid residue (Figure 6b). Notably, the absence of the band for the La^{3+}-bound sample indicates that the bidentate coordination is disrupted. In addition, the difference spectrum for the Ca^{2+}-bound CaM shows greater crossband intensity than for La^{3+}-bound CaM or apoprotein. This crossband intensity results from vibrational energy transfer among side chains and the amide backbone and suggests that the binding site is more rigid when Ca^{2+} rather than La^{3+} is bound. Consistent with disorder in La^{3+}-bound CaM, the 2D amide

band in the spectrum for La^{3+}-bound CaM taken with long T_w is more elongated along the diagonal, indicative of greater inhomogeneity with slow dynamics. Thus, through several features, 2D IR distinguishes CaM recognition of Ca^{2+} and La^{3+}.

Residue-specific characterization of CaM recognition.—The same CaM domain has been investigated more globally by 2D IR through the introduction of nonnative vibrational probes (92). In addition to Ca^{2+} binding, the study considered CaM recognition of a peptide ligand (Figure 7a). Distinct locations in CaM were characterized by mutation of residues to cysteine, then cyanylation to introduce thiocyanate probes as thiocyanocysteine (*CN*SCys) residues. The probes were placed at a conserved native isoleucine in the Ca^{2+}-binding site (*CN*SCys100), conserved native methionine residues that contact the peptide ligand (*CN*SCys72, *CN*SCys109, and *CN*SCys145), and a solvent-exposed control site in the ion recognition domain (*CN*SCys17).

T_w-dependent 2D spectra exhibit elongation along the diagonal that indicates inhomogeneous broadening (Figure 7b). The lineshapes evolve with increasing T_w due to the interconversion among the underlying states. A metric for the spectral elongation, the CLS, is plotted on the 2D bands. The CLS decays with T_w reveal how the sensitivity of the dynamics to binding Ca^{2+} or the peptide ligand varies among locations in CaM (Figure 7c). The probe near the ion-binding site (*CN*SCys100) is sensitive to binding Ca^{2+} but responds modestly to peptide binding. In contrast, probes involved in peptide ligand recognition (*CN*SCys72, *CN*SCys109, and *CN*SCys145) are sensitive to binding the peptide but not Ca^{2+}. The data report on the varying involvement of different locations in two aspects of the functional mechanism of CaM. Additionally, this study exemplifies the current sensitivity of protein 2D IR and temporal extent of measurement of equilibrium dynamics with nonnative side chain probes.

Enzymatic selectivity.—The cytochrome P450 (P450) superfamily of heme oxidases catalyze diverse biosynthetic and metabolic reactions (134). Regioselectivity of P450 catalysis, at which site(s) on a substrate are oxidized, depends on the orientation of a substrate in the active site and whether carbon centers can approach a reactive oxy-heme intermediate. For example, the high (100%) regioselectivity of hydroxylation of the substrate camphor by the archetypical P450, P450cam, is attributed to rigid packing that restricts substrate mobility (135). Camphor binding triggers a conformational change by P450cam from an open to closed state in which a helix-loop-helix motif (F/G helices) packs onto the active site (136) (Figure 8a).

To investigate how protein dynamics contribute to regioselectivity, 2D IR was applied to compare the binding by P450cam of camphor and another substrate, norcamphor, which yields two major hydroxylation products (93). *CN*F was incorporated to probe along the interface of the F/G helices (*CN*F201, *CN*F98, *CN*F87), toward the substrate (*CN*F96), and toward solvent (*CN*F305). Variance among 1D spectra and CLS decays reveal the heterogeneous response of the locations in P450cam to substrate binding, and moreover, the distinct impact of binding camphor versus norcamphor (Figure 8b,c). Probes placed at the interface of the F/G helices (*CN*F87, *CN*F98, and *CN*F201) reflect sensitivity to the conformational change induced by camphor binding. In contrast, norcamphor binding results

in no response (*CN*F201, *CN*F98) or a diminished response (*CN*F87). Whereas *CN*F87 for the camphor complex shows a single band, the asymmetric lineshape for the norcamphor complex indicates a second populated state (Figure 8b). Interconversion between these states corresponds with slower dynamics in the norcamphor complex (Figure 8c). Similarly, *CN*F96, which is directed at substrate, shows a single band for the camphor complex, but two in the norcamphor complex. However, for *CN*F96, the states in the norcamphor complex interconvert rapidly. In agreement, 2D IR of a CO heme ligand, which also contacts the bound substrate, reports faster dynamics in the norcamphor than camphor complex (51). The rapid dynamics are consistent with the timescale of transitioning orientations of norcamphor that would result in multiple hydroxynorcamphor products. Altogether, the spectral data illuminate how norcamphor binding does not fully induce the conformational transition to the closed state of P450cam, while rapid dynamics persist within the active site.

OUTLOOK

Since the first demonstrations about two decades ago, 2D IR is expanding from fundamental research of simple molecules to analytical methods that can tackle complex systems. The complexity of samples feasible for 2D IR is exemplified by studies of cataract protein in tissue samples (122). Amide 2D IR for analysis of protein secondary structure has been demonstrated in complex mixtures and in H_2O rather than D_2O, eliminating the need for the time-consuming sample preparation (137, 138). Methods have been described to standardize analysis using the thermal response of water as an internal standard to normalize 2D protein spectra and enable accurate and precise determination of protein concentration by different instruments and laboratories (139). 2D IR of immunocaptured proteins on surfaces implemented in attenuated total reflection mode can take advantage of plasmonic signal enhancement (128). Further technological development will improve detection limits and analysis throughput.

Efforts are ongoing to expand and improve the assortment of vibrational probes for 2D IR of proteins. Accessing slower timescale equilibrium dynamics motivates design of probes with longer vibrational lifetimes. Isotope labeling has been explored to detune vibrations from accepting modes, which has resulted in a modest (~2-fold) increase in lifetime (105, 140). Another strategy is to decouple the probe from intermolecular relaxation pathways by insertion of heavy atoms (141–144). The insertion of sulfur to decouple the cyano vibration in the *CNS* probe described above is an example. Insertion of a selenium atom to decouple vibrations has also been explored. For example, in comparison to *CN*F, the cyano vibration of cyanoselenophenylalanine shows a greatly (>50-fold) extended lifetime (143). The next step for this and other probes is to develop efficient methods for selective incorporation into proteins.

Protein dynamics range in scale from an individual amino acid to global domain conformations to protein–protein interactions. We are only beginning to understand the connections between these spatial levels. Protein 2D IR has started to address the question through characterization of multiple local or delocalized vibrations within a protein. For example, studies highlighted above obtained multiple views of global and local dynamics from nonnative vibrational probes at various locations of CaM and P450cam, carboxylate

side chain and amide backbone vibrations of CaM, and amide spectral signatures of secondary structure and dimerization of insulin. Continued expansion of 2D IR using multiple vibrational modes to correlate dynamics among scales will further uncover their connections. These efforts will be bolstered by developments in generation of intense broadband IR pulses to span wide spectral ranges (145–147).

Further development of 2D IR instrumentation and protein labeling methodology to improve sensitivity and selectivity should enable access to larger, more complex targets and expand the techniques in analytical chemistry and other fields of research. In principle, 2D IR has no size restrictions for characterization of proteins or multiprotein complexes. Membrane proteins are generally less understood than soluble proteins and are important future targets. Expansion of 2D IR for nucleic acids currently lags in comparison to proteins but could provide critical insight into functional dynamics of flexible RNA macromolecules (148–150). Sugars and protein glycosylation are now recognized as critically important in cellular biochemistry but not yet subjects of study by 2D IR. Biomolecular 2D IR is poised for exciting applications ahead.

SUMMARY

2D IR is emerging as a powerful approach for analysis of protein structure and dynamics. The additional information provided by the second dimension facilitates interpretation of complex protein spectra. The methods can probe local and global dynamics at the backbone, side chains, or ligands. 2D IR captures rapidly interconverting states and directly measures rapid equilibrium dynamics or slower kinetics of folding, aggregation, and potentially many other processes. We briefly touched upon a few examples that illustrate the diverse applications of 2D IR to examine functional protein dynamics. A rich toolbox of 2D IR methods provides versatile approaches for characterizing a wide variety of biomolecular samples and addressing diverse questions about the biophysics of their function.

ACKNOWLEDGMENTS

The authors are thankful for support from Indiana University, the Department of Energy (DE-SC0018983), National Science Foundation (1552996), and National Institutes of Health (GM114500).

DISCLOSURE STATEMENT

The authors are not aware of any affiliations, memberships, funding, or financial holdings that might be perceived as affecting the objectivity of this review.

LITERATURE CITED

1. Frauenfelder H, Sligar SG, Wolynes PG. 1991. The energy landscapes and motions of proteins. Science 254:1598–1603 [PubMed: 1749933]
2. Wei G, Xi W, Nussinov R, Ma B. 2016. Protein ensembles: How does nature harness thermodynamic fluctuations for life? The diverse functional roles of conformational ensembles in the cell. Chem. Rev 116:6516–51 [PubMed: 26807783]
3. Campitelli P, Modi T, Kumar S, Ozkan SB. 2020. The role of conformational dynamics and allostery in modulating protein evolution. Annu. Rev. Biophys 49:267–88 [PubMed: 32075411]
4. Ganim Z, Hoi SC, Smith AW, DeFlores LP, Jones KC, Tokmakoff A. 2008. Amide I two-dimensional infrared spectroscopy of proteins. Acc. Chem. Res 41:432–41 [PubMed: 18288813]

5. Kim YS, Hochstrasser RM. 2009. Applications of 2D IR spectroscopy to peptides, proteins, and hydrogen-bond dynamics. J. Phys. Chem. B 113:8231–51 [PubMed: 19351162]
6. Hunt NT. 2009. 2D-IR spectroscopy: ultrafast insights into biomolecule structure and function. Chem. Soc. Rev 38:1837–48 [PubMed: 19551165]
7. Le Sueur AL, Horness RE, Thielges MC. 2015. Applications of two-dimensional infrared spectroscopy. Analyst 140:4336–49 [PubMed: 26007625]
8. Ghosh A, Ostrander JS, Zanni MT. 2017. Watching proteins wiggle: mapping structures with two-dimensional infrared spectroscopy. Chem. Rev 117:10726–59 [PubMed: 28060489]
9. Adhikary R, Zimmermann J, Romesberg FE. 2017. Transparent window vibrational probes for the characterization of proteins with high structural and temporal resolution. Chem. Rev 117:1927–69 [PubMed: 28106985]
10. Hamm P, Lim M, Degrado WF, Hochstrasser RM. 1999. The two-dimensional IR nonlinear spectroscopy of a cyclic penta-peptide in relation to its three-dimensional structure. PNAS 96:2036–41 [PubMed: 10051590]
11. Mukamel S 1995. Principles of Nonlinear Optical Spectroscopy. New York: Oxford Univ. Press
12. Hamm P, Zanni M. 2011. Concepts and Methods of 2D Infrared Spectroscopy. Cambridge, UK: Cambridge Univ. Press
13. Park S, Kwak K, Fayer MD. 2007. Ultrafast 2D-IR vibrational echo spectroscopy: a probe of molecular dynamics. Laser Phys. Lett 4:704–18
14. Baiz CR, Błasiak B, Bredenbeck J, Cho M, Choi J-H, et al. 2020. Vibrational spectroscopic map, vibrational spectroscopy, and intermolecular interaction. Chem. Rev 120:7152–218 [PubMed: 32598850]
15. Merchant KA, Thompson DE, Fayer MD. 2001. Two-dimensional time-frequency ultrafast infrared vibrational echo spectroscopy. Phys. Rev. Lett 86:3899–902 [PubMed: 11329352]
16. Zanni MT, Hochstrasser RM. 2001. Two-dimensional infrared spectroscopy: a promising new method for the time resolution of structures. Curr. Opin. Struct. Biol 11:516–22 [PubMed: 11785750]
17. Cervetto V, Helbing J, Bredenbeck J, Hamm P. 2004. Double-resonance versus pulsed Fourier transform two-dimensional infrared spectroscopy: an experimental and theoretical comparison. J. Chem. Phys 121:5935–42 [PubMed: 15367022]
18. DeFlores LP, Nicodemus RA, Tokmakoff A. 2007. Two-dimensional Fourier transform spectroscopy in the pump-probe geometry. Opt. Lett 32:2966–68 [PubMed: 17938668]
19. Shim SH, Strasfeld DB, Ling YL, Zanni MT. 2007. Automated 2D IR spectroscopy using a mid-IR pulse shaper and application of this technology to the human islet amyloid polypeptide. PNAS 104:14197–202 [PubMed: 17502604]
20. Bloem R, Garrett-Roe S, Strzalka H, Hamm P, Donaldson P 2010. Enhancing signal detection and completely eliminating scattering using quasi-phase-cycling in 2D IR experiments. Opt. Express 18:27067–78 [PubMed: 21196983]
21. Karthick Kumar SK, Tamimi A, Fayer MD. 2012. Comparisons of 2D IR measured spectral diffusion in rotating frames using pulse shaping and in the stationary frame using the standard method. J. Chem. Phys 137:184201 [PubMed: 23163363]
22. Rock W, Li YL, Pagano P, Cheatum CM. 2013. 2D IR spectroscopy using four-wave mixing, pulse shaping, and IR upconversion: a quantitative comparison. J. Phys. Chem. A 117:6073–83 [PubMed: 23687988]
23. Ghosh A, Serrano AL, Oudenhoven TA, Ostrander JS, Eklund EC, et al. 2016. Experimental implementations of 2D IR spectroscopy through a horizontal pulse shaper design and a focal plane array detector. Opt. Lett 41:524–27 [PubMed: 26907414]
24. Backus EHG, Garrett-Roe S, Hamm P 2008. Phasing problem of heterodyne-detected two-dimensional infrared spectroscopy. Opt. Lett 33:2665–67 [PubMed: 19015702]
25. Bristow AD, Karaiskaj D, Dai X, Cundiff ST. 2008. All-optical retrieval of the global phase for two-dimensional Fourier-transform spectroscopy. Opt. Express 16:18017–27 [PubMed: 18958080]
26. Middleton CT, Strasfeld DB, Zanni MT. 2009. Polarization shaping in the mid-IR and polarization-based balanced heterodyne detection with application to 2D IR spectroscopy. Opt. Express 17:14526–33 [PubMed: 19687931]

27. Osborne DG, Kubarych KJ. 2013. Rapid and accurate measurement of the frequency-frequency correlation function. J. Phys. Chem. A 117:5891–98 [PubMed: 23231628]
28. Kramer PL, Giammanco CH, Tamimi A, Hoffman DJ, Sokolowsky KP, Fayer MD. 2016. Quasi-rotating frame: accurate line shape determination with increased efficiency in noncollinear 2D optical spectroscopy. J. Opt. Soc. Am. B 33:1143–56
29. Lomont JP, Ostrander JS, Ho J-J, Petti MK, Zanni MT. 2017. Not all β-sheets are the same: amyloid infrared spectra, transition dipole strengths, and couplings investigated by 2D IR spectroscopy. J. Phys. Chem. B 121:8935–45 [PubMed: 28851219]
30. Grechko M, Zanni MT. 2012. Quantification of transition dipole strengths using 1D and 2D spectroscopy for the identification of molecular structures via exciton delocalization: application to α-helices. J. Chem. Phys 137:184202 [PubMed: 23163364]
31. Dunkelberger EB, Grechko M, Zanni MT. 2015. Transition dipoles from 1D and 2D infrared spectroscopy help reveal the secondary structures of proteins: application to amyloids. J. Phys. Chem. B 119:14065–75 [PubMed: 26446575]
32. Ramos S, Basom EJ, Thielges MC. 2018. Conformational change induced by putidaredoxin binding to ferrous CO-ligated cytochrome P450cam characterized by 2D IR spectroscopy. Front. Mol. Biosci 5:94 [PubMed: 30483514]
33. Kim H, Cho M. 2013. Infrared probes for studying the structure and dynamics of biomolecules. Chem. Rev 113:5817–47 [PubMed: 23679868]
34. Kwak K, Park S, Finkelstein IJ, Fayer M. 2007. Frequency-frequency correlation functions and apodization in two-dimensional infrared vibrational echo spectroscopy: a new approach. J. Chem. Phys 127:124503 [PubMed: 17902917]
35. Kwak K, Rosenfeld DE, Fayer MD. 2008. Taking apart the two-dimensional infrared vibrational echo spectra: more information and elimination of distortions. J. Chem. Phys 128:204505 [PubMed: 18513030]
36. Ishikawa H, Kwak K, Chung JK, Kim S, Fayer MD. 2008. Direct observation of fast protein conformational switching. PNAS 105:8619–24 [PubMed: 18562286]
37. Tokmakoff A 2000. Two-dimensional line shapes derived from coherent third-order nonlinear spectroscopy. J. Phys. Chem. A 104:4247–55
38. Demirdöven N, Khalil M, Tokmakoff A. 2002. Correlated vibrational dynamics revealed by two-dimensional infrared spectroscopy. Phys. Rev. Lett 89:237401 [PubMed: 12485039]
39. Asbury JB, Steinel T, Stromberg C, Corcelli SA, Lawrence CP, et al. 2004. Water dynamics: vibrational echo correlation spectroscopy and comparison to molecular dynamics simulations. J. Phys. Chem. A 108:1107–19
40. Roberts ST, Loparo JJ, Tokmakoff A. 2006. Characterization of spectral diffusion from two-dimensional line shapes. J. Chem. Phys 125:084502 [PubMed: 16965024]
41. Eaves JD, Loparo JJ, Fecko CJ, Roberts ST, Tokmakoff A, Geissler PL. 2005. Hydrogen bonds in liquid water are broken only fleetingly. PNAS 102:13019–22 [PubMed: 16135564]
42. Kwac K, Cho M. 2003. Two-color pump–probe spectroscopies of two- and three-level systems:2-dimensional line shapes and solvation dynamics. J. Phys. Chem. A 107:5903–12
43. Golonzka O, Tokmakoff A. 2001. Polarization-selective third-order spectroscopy of coupled vibronic states. J. Chem. Phys 115:297–309
44. Zanni MT, Ge N-H, Kim YS, Hochstrasser RM. 2001. Two-dimensional IR spectroscopy can be designed to eliminate the diagonal peaks and expose only the crosspeaks needed for structure determination. PNAS 98:11265–70 [PubMed: 11562493]
45. Chalyavi F, Gilmartin PH, Schmitz AJ, Fennie MW, Tucker MJ. 2018. Synthesis of 5-cyano-tryptophan as a two-dimensional infrared spectroscopic reporter of structure. Angew. Chem. Int. Ed 57:7528–32
46. Merchant KA, Thompson DE, Xu Q-H, Williams RB, Loring RF, Fayer MD. 2002. Myoglobin-CO conformational substate dynamics: 2D vibrational echoes and MD simulations. Biophys. J 82:3277–88 [PubMed: 12023251]
47. Merchant KA, Noid WG, Akiyama R, Finkelstein IJ, Goun A, et al. 2003. Myoglobin-CO substate structures and dynamics: multidimensional vibrational echoes and molecular dynamics simulations. J. Am. Chem. Soc 125:13804–18 [PubMed: 14599220]

48. Thielges MC, Fayer MD. 2012. Protein dynamics studied with ultrafast two-dimensional infrared vibrational echo spectroscopy. Acc. Chem. Res 45:1866–74 [PubMed: 22433178]
49. Maj M, Oh Y, Park K, Lee J, Kwak KW, Cho M. 2014. Vibrational dynamics of thiocyanate and selenocyanate bound to horse heart myoglobin. J. Chem. Phys 140:235104 [PubMed: 24952571]
50. Van Wilderen LJGW, Kern-Michler D, Müller-Werkmeister HM, Bredenbeck J. 2014. Vibrational dynamics and solvatochromism of the label SCN in various solvents and hemoglobin by time dependent IR and 2D-IR spectroscopy. Phys. Chem. Chem. Phys 16:19643–53 [PubMed: 25111557]
51. Basom EJ, Spearman JW, Thielges MC. 2015. Conformational landscape and the selectivity of cytochrome P450cam. J. Phys. Chem. B 119:6620–27 [PubMed: 25955684]
52. Maj M, Kwak K, Cho M. 2015. Ultrafast structural fluctuations of myoglobin-bound thiocyanate and selenocyanate ions measured with two-dimensional infrared photon echo spectroscopy. Chem. Phys. Chem 16:3468–76 [PubMed: 26359112]
53. Horch M, Schoknecht J, Wrathall SLD, Greetham GM, Lenz O, Hunt NT. 2019. Understanding the structure and dynamics of hydrogenases by ultrafast and two-dimensional infrared spectroscopy. Chem. Sci 10:8981–89 [PubMed: 31762978]
54. Fang C, Bauman JD, Das K, Remorino A, Arnold E, Hochstrasser RM. 2007. Two-dimensional infrared spectra reveal relaxation of the nonnucleoside inhibitor TMC278 complexed with HIV-1 reverse transcriptase. PNAS 105:1472–77 [PubMed: 18040050]
55. Bandaria JN, Dutta S, Hill SE, Kohen A, Cheatum CM. 2008. Fast enzyme dynamics at the active site of formate dehydrogenase. J. Am. Chem. Soc 130:22–23 [PubMed: 18067303]
56. Bandaria JN, Dutta S, Nydegger MW, Rock W, Kohen A, Cheatum CM. 2010. Characterizing the dynamics of functionally relevant complexes of formate dehydrogenase. PNAS 107:17974–79 [PubMed: 20876138]
57. Pagano P, Guo Q, Kohen A, Cheatum CM. 2016. Oscillatory enzyme dynamics revealed by two-dimensional infrared spectroscopy. J. Phys. Chem. Lett 7:2507–11 [PubMed: 27305279]
58. Demirdöven N, Cheatum CM, Chung HS, Khalil M, Knoester J, Tokmakoff A. 2004. Two-dimensional infrared spectroscopy of antiparallel β-sheet secondary structure. J. Am. Chem. Soc 126:7981–90 [PubMed: 15212548]
59. Maekawa H, Poli MD, Moretto A, Toniolo C, Ge N-H. 2009. Toward detecting the formation of a single helical turn by 2D IR cross peaks between the amide-I and -II modes. J. Phys. Chem. B 113:11775–86 [PubMed: 19642666]
60. DeFlores LP, Ganim Z, Nicodemus RA, Tokmakoff A. 2009. Amide I′–II′ 2D IR spectroscopy provides enhanced protein secondary structural sensitivity. J. Am. Chem. Soc 131:3385–91 [PubMed: 19256572]
61. Buchanan LE, Dunkelberger EB, Tran HQ, Cheng P-N, Chiu C-C, et al. 2013. Mechanism of IAPP amyloid fibril formation involves an intermediate with a transient β-sheet. PNAS 110:19285–90 [PubMed: 24218609]
62. Stevenson P, Tokmakoff A. 2015. Distinguishing gramicidin D conformers through two-dimensional infrared spectroscopy of vibrational excitons. J. Chem. Phys 142:212424 [PubMed: 26049444]
63. Zhang X-X, Jones KC, Fitzpatrick A, Peng CS, Feng C-J, et al. 2016. Studying protein–protein binding through T-jump induced dissociation: transient 2D IR spectroscopy of insulin dimer. J. Phys. Chem. B 120:5134–45 [PubMed: 27203447]
64. Woutersen S, Pfister R, Hamm P, Mu Y, Kosov DS, Stock G. 2002. Peptide conformational heterogeneity revealed from nonlinear vibrational spectroscopy and molecular-dynamics simulations. J. Chem. Phys 117:6833–40
65. Fang C, Senes A, Cristian L, DeGrado WF, Hochstrasser RM. 2006. Amide vibrations are delocalized across the hydrophobic interface of a transmembrane helix dimer. PNAS 103:16740–45 [PubMed: 17075037]
66. Remorino A, Hochstrasser RM. 2012. Three-dimensional structures by two-dimensional vibrational spectroscopy. Acc. Chem. Res 45:1896–905 [PubMed: 22458539]

67. Kratochvil HT, Carr JK, Matulef K, Annen AW, Li H, et al. 2016. Instantaneous ion configurations in the K^+ ion channel selectivity filter revealed by 2D IR spectroscopy. Science 353:1040–44 [PubMed: 27701114]
68. Andresen ER, Hamm P 2009. Site-specific difference 2D-IR spectroscopy of bacteriorhodopsin. J. Phys. Chem. B 113:6520–27 [PubMed: 19358550]
69. Edington SC, Gonzalez A, Middendorf TR, Halling DB, Aldrich RW, Baiz CR. 2018. Coordination to lanthanide ions distorts binding site conformation in calmodulin. PNAS 115:E3126–34 [PubMed: 29545272]
70. Torres J, Kukol A, Goodman JM, Arkin IT. 2001. Site-specific examination of secondary structure and orientation determination in membrane proteins: the peptidic $^{13}C=^{18}O$ group as a novel infrared probe. Biopolymers 59:396–401 [PubMed: 11598874]
71. Mukherjee P, Kass I, Arkin IT, Arkin I, Zanni MT. 2006. Picosecond dynamics of a membrane protein revealed by 2D IR. PNAS 103:3528–33 [PubMed: 16505377]
72. Backus EHG, Bloem R, Donaldson PM, Ihalainen JA, Pfister R, et al. 2010. 2D-IR study of a photoswitchable isotope-labeled α-helix. J. Phys. Chem. B 114:3735–40 [PubMed: 20166694]
73. Moran SD, Woys AM, Buchanan LE, Bixby E, Decatur SM, Zanni MT. 2012. Two-dimensional IR spectroscopy and segmental ^{13}C labeling reveals the domain structure of human γD-crystallin amyloid fibrils. PNAS 109:3329–34 [PubMed: 22328156]
74. Maj M, Lomont JP, Rich KL, Alperstein AM, Zanni MT. 2018. Site-specific detection of protein secondary structure using 2D IR dihedral indexing: a proposed assembly mechanism of oligomeric hIAPP Chem. Sci 9:463–74 [PubMed: 29619202]
75. Abaskharon RM, Brown SP, Zhang W, Chen J, Smith AB, Gai F. 2017. Isotope-labeled aspartate sidechain as a non-perturbing infrared probe: application to investigate the dynamics of a carboxylate buried inside a protein. Chem. Phys. Lett 683:193–98 [PubMed: 29033461]
76. Kozinski M, Garrett-Roe S, Hamm P 2008. 2D-IR spectroscopy of the sulfhydryl band of cysteines in the hydrophobic core of proteins. J. Phys. Chem. B 112:7645–50 [PubMed: 18512974]
77. Chalyavi F, Hogle DG, Tucker MJ. 2017. Tyrosine as a non-perturbing site-specific vibrational reporter for protein dynamics. J. Phys. Chem. B 121:6380–89 [PubMed: 28590738]
78. Ghosh A, Tucker MJ, Hochstrasser RM. 2011. Identification of arginine residues in peptides by 2D-IR echo spectroscopy. J. Phys. Chem. A 115:9731–38 [PubMed: 21539337]
79. Huerta-Viga A, Amirjalayer S, Domingos SR, Meuzelaar H, Rupenyan A, Woutersen S. 2015. The structure of salt bridges between Arg^+ and Glu^- in peptides investigated with 2D-IR spectroscopy: evidence for two distinct hydrogen-bond geometries. J. Chem. Phys 142:212444 [PubMed: 26049464]
80. Thielges MC, Axup JY, Wong D, Lee HS, Chung JK, et al. 2011. Two-dimensional IR spectroscopy of protein dynamics using two vibrational labels: a site-specific genetically encoded unnatural amino acid and an active site ligand. J. Phys. Chem. B 115:11294–304 [PubMed: 21823631]
81. King JT, Kubarych KJ. 2012. Site-specific coupling of hydration water and protein flexibility studied in solution with ultrafast 2D-IR spectroscopy. J. Am. Chem. Soc 134:18705–12 [PubMed: 23101613]
82. King JT, Arthur EJ, Brooks CL, Kubarych KJ. 2012. Site-specific hydration dynamics of globular proteins and the role of constrained water in solvent exchange with amphiphilic cosolvents. J. Phys. Chem. B 116:5604–11 [PubMed: 22530969]
83. Bloem R, Koziol K, Waldauer SA, Buchli B, Walser R, et al. 2012. Ligand binding studied by 2D IR spectroscopy using the azidohomoalanine label. J. Phys. Chem. B 116:13705–12 [PubMed: 23116486]
84. Woys AM, Mukherjee SS, Skoff DR, Moran SD, Zanni MT. 2013. A strongly absorbing class of nonnatural labels for probing protein electrostatics and solvation with FTIR and 2D IR spectroscopies. J. Phys. Chem. B 117:5009–18 [PubMed: 23537223]
85. King JT, Arthur EJ, Brooks CL 3rd, Kubarych KJ. 2014. Crowding induced collective hydration of biological macromolecules over extended distances. J. Am. Chem. Soc 136:188–94 [PubMed: 24341684]

86. Ross MR, White AM, Yu F, King JT, Pecoraro VL, Kubarych KJ. 2015. Histidine orientation modulates the structure and dynamics of a de novo metalloenzyme active site. J. Am. Chem. Soc 137:10164–76 [PubMed: 26247178]
87. Stucki-Buchli B, Johnson PJM, Bozovic O, Zanobini C, Koziol KL, et al. 2017. 2D-IR spectroscopy of an AHA labeled photoswitchable PDZ2 domain. J. Phys. Chem. A 121:9435–45 [PubMed: 29160709]
88. Johnson PJM, Koziol KL, Hamm P 2017. Quantifying biomolecular recognition with site-specific 2D infrared probes. J. Phys. Chem. Lett 8:2280–84 [PubMed: 28471671]
89. Zanobini C, Bozovic O, Jankovic B, Koziol KL, Johnson PJM, et al. 2018. Azidohomoalanine: a minimally invasive, versatile, and sensitive infrared label in proteins to study ligand binding. J. Phys. Chem. B 122:10118–25 [PubMed: 30343570]
90. Ramos S, Le Sueur AL, Horness RE, Specker JT, Collins JA, et al. 2019. Heterogeneous and highly dynamic interface in plastocyanin-cytochrome F complex revealed by site-specific 2D-IR spectroscopy. J. Phys. Chem. B 123:2114–22 [PubMed: 30742428]
91. Ramos S, Horness RE, Collins JA, Haak D, Thielges MC. 2019. Site-specific 2D IR spectroscopy: a general approach for the characterization of protein dynamics with high spatial and temporal resolution. Phys. Chem. Chem. Phys 21:780–88 [PubMed: 30548035]
92. Schmidt-Engler JM, Zangl R, Guldan P, Morgner N, Bredenbeck J. 2020. Exploring the 2D-IR repertoire of the –SCN label to study site-resolved dynamics and solvation in the calcium sensor protein calmodulin. Phys. Chem. Chem. Phys 22:5463–75 [PubMed: 32096510]
93. Ramos S, Mammoser CC, Thibodeau KE, Thielges MC. 2021. Dynamics underlying hydroxylation selectivity of cytochrome P450cam. Biophys. J 120:912–23 [PubMed: 33545101]
94. Merrifield RB. 1963. Solid phase peptide synthesis. I. The synthesis of a tetrapeptide. J. Am. Chem. Soc 85:2149–54
95. Chung JK, Thielges MC, Fayer MD. 2012. Conformational dynamics and stability of HP35 studied with 2D IR vibrational echoes. J. Am. Chem. Soc 134:12118–24 [PubMed: 22764745]
96. Chung JK, Thielges MC, Lynch SR, Fayer MD. 2012. Fast dynamics of HP35 for folded and urea-unfolded conditions. J. Phys. Chem. B 116:11024–31 [PubMed: 22909017]
97. Urbanek DC, Vorobyev DY, Serrano AL, Gai F, Hochstrasser RM. 2010. The two dimensional vibrational echo of a nitrile probe of the villin HP35 protein. J. Phys. Chem. Lett 1:3311–15 [PubMed: 21132120]
98. Bagchi S, Boxer SG, Fayer MD. 2012. Ribonuclease S dynamics measured using a nitrile label with 2D IR vibrational echo spectroscopy. J. Phys. Chem. B 116:4034–42 [PubMed: 22417088]
99. Beligere GS, Dawson PE. 1999. Conformationally assisted protein ligation using C-terminal thioester peptides. J. Am. Chem. Soc 121:6332–33
100. Dawson PE, Kent SBH. 2000. Synthesis of native proteins by chemical ligation. Annu. Rev. Biochem 69:923–60 [PubMed: 10966479]
101. Muir TW 2003. Semisynthesis of proteins by expressed protein ligation. Annu. Rev. Biochem 72:249–89 [PubMed: 12626339]
102. Fafarman AT, Webb LJ, Chuang JI, Boxer SG. 2006. Site-specific conversion of cysteine thiols into thiocyanate creates an IR probe for electric fields in proteins. J. Am. Chem. Soc 128:13356–57 [PubMed: 17031938]
103. Liu CC, Schultz PG. 2010. Adding new chemistries to the genetic code. Annu. Rev. Biochem 79:413–44 [PubMed: 20307192]
104. Peuker S, Andersson H, Gustavsson E, Maiti KS, Kania R, et al. 2016. Efficient isotope editing of proteins for site-directed vibrational spectroscopy. J. Am. Chem. Soc 138:2312–18 [PubMed: 26796542]
105. Park JY, Kwon H-J, Mondal S, Han H, Kwak K, Cho M. 2020. Two-dimensional IR spectroscopy reveals a hidden Fermi resonance band in the azido stretch spectrum of β-azidoalanine. Phys. Chem. Chem. Phys 22:19223–29 [PubMed: 32812969]
106. Schmidt-Engler JM, Blankenburg L, Błasiak B, van Wilderen LJGW, Cho M, Bredenbeck J. 2020. Vibrational lifetime of the SCN protein label in H_2O and D_2O reports site-specific solvation and structure changes during PYP's photocycle. Anal. Chem 92:1024–32 [PubMed: 31769286]

107. Chung HS, Khalil M, Tokmakoff A. 2004. Nonlinear infrared spectroscopy of protein conformational change during thermal unfolding. J. Phys. Chem. B 108:15332–42
108. Huerta-Viga A, Woutersen S. 2013. Protein denaturation with guanidinium: a 2D-IR study. J. Phys. Chem. Lett 4:3397–401 [PubMed: 24163724]
109. Minnes L, Shaw DJ, Cossins BP, Donaldson PM, Greetham GM, et al. 2017. Quantifying secondary structure changes in calmodulin using 2D-IR spectroscopy. Anal. Chem 89:10898–906 [PubMed: 28921967]
110. Chung HS, Khalil M, Smith AW, Ganim Z, Tokmakoff A. 2005. Conformational changes during the nanosecond-to-millisecond unfolding of ubiquitin. PNAS 102:612–17 [PubMed: 15630083]
111. Kolano C, Helbing J, Kozinski M, Sander W, Hamm P. 2006. Watching hydrogen-bond dynamics in a β-turn by transient two-dimensional infrared spectroscopy. Nature 444:469–72 [PubMed: 17122853]
112. Causgrove TP, Dyer RB. 2006. Nonequilibrium protein folding dynamics: laser-induced pH-jump studies of the helix–coil transition. Chem. Phys 323:2–10
113. Chung HS, Ganim Z, Jones KC, Tokmakoff A. 2007. Transient 2D IR spectroscopy of ubiquitin unfolding dynamics. PNAS 104:14237–42 [PubMed: 17551015]
114. Tucker MJ, Abdo M, Courter JR, Chen J, Brown SP, et al. 2013. Nonequilibrium dynamics of helix reorganization observed by transient 2D IR spectroscopy. PNAS 110:17314–19 [PubMed: 24106309]
115. Meuzelaar H, Panman MR, Woutersen S. 2015. Guanidinium-induced denaturation by breaking of salt bridges. Angew. Chem. Int. Ed 54:15255–59
116. Stevenson P, Tokmakoff A. 2017. Time-resolved measurements of an ion channel conformational change driven by a membrane phase transition. PNAS 114:10840–45 [PubMed: 28973859]
117. Chiti F, Dobson CM. 2006. Protein misfolding, functional amyloid, and human disease. Annu. Rev. Biochem 75:333–66 [PubMed: 16756495]
118. Shim SH, Gupta R, Ling YL, Strasfeld DB, Raleigh D, Zanni MT. 2009. Two-dimensional IR spectroscopy and isotope labeling defines the pathway of amyloid formation with residue-specific resolution. PNAS 106:6614–19 [PubMed: 19346479]
119. Ling YL, Strasfeld DB, Shim SH, Raleigh DP, Zanni MT. 2009. Two-dimensional infrared spectroscopy provides evidence of an intermediate in the membrane-catalyzed assembly of diabetic amyloid. J. Phys. Chem. B 113:2498–505 [PubMed: 19182939]
120. Dunkelberger EB, Buchanan LE, Marek P, Cao P, Raleigh DP, Zanni MT. 2012. Deamidation accelerates amyloid formation and alters amylin fiber structure. J. Am. Chem. Soc 134:12658–67 [PubMed: 22734583]
121. Iyer A, Roeters SJ, Schilderink N, Hommersom B, Heeren RMA, et al. 2016. The impact of N-terminal acetylation of α-synuclein on phospholipid membrane binding and fibril structure. J. Biol. Chem 291:21110–22 [PubMed: 27531743]
122. Zhang TO, Alperstein AM, Zanni MT. 2017. Amyloid β-sheet secondary structure identified in UV-induced cataracts of porcine lenses using 2D IR spectroscopy. J. Mol. Biol 429:1705–21 [PubMed: 28454743]
123. Roeters SJ, Sawall M, Eskildsen CE, Panman MR, Tordai G, et al. 2020. Unraveling vealyl amyloid formation using advanced vibrational spectroscopy and microscopy. Biophys. J 119:87–98 [PubMed: 32562617]
124. Fields CR, Dicke SS, Petti MK, Zanni MT, Lomont JP. 2020. A different hIAPP polymorph is observed in human serum than in aqueous buffer: demonstration of a new method for studying amyloid fibril structure using infrared spectroscopy. J. Phys. Chem. Lett 11:6382–88 [PubMed: 32706257]
125. Iyer A, Roeters SJ, Kogan V, Woutersen S, Claessens MMAE, Subramaniam V 2017. C-terminal truncated α-synuclein fibrils contain strongly twisted β-sheets. J. Am. Chem. Soc 139:15392–400 [PubMed: 28968082]
126. Buchanan LE, Maj M, Dunkelberger EB, Cheng P-N, Nowick JS, Zanni MT. 2018. Structural polymorphs suggest competing pathways for the formation of amyloid fibrils that diverge from a common intermediate species. Biochemistry 57:6470–78 [PubMed: 30375231]

127. Lomont JP, Rich KL, Maj M, Ho J-J, Ostrander JS, Zanni MT. 2018. Spectroscopic signature for stable β-amyloid fibrils versus β-sheet-rich oligomers. J. Phys. Chem. B 122:144–53 [PubMed: 29220175]
128. Ostrander JS, Lomont JP, Rich KL, Saraswat V, Feingold BR, et al. 2019. Monolayer sensitivity enables a 2D IR spectroscopic immuno-biosensor for studying protein structures: application to amyloid polymorphs. J. Phys. Chem. Lett 10:3836–42 [PubMed: 31246039]
129. Roeters SJ, Iyer A, Pletikapiä G, Kogan V, Subramaniam V, Woutersen S. 2017. Evidence for intramolecular antiparallel beta-sheet structure in alpha-synuclein fibrils from a combination of two-dimensional infrared spectroscopy and atomic force microscopy. Sci. Rep 7:41051 [PubMed: 28112214]
130. Coates L 2020. Ion permeation in potassium ion channels. Acta Crystallogr. D Struct. Biol 76:326–31 [PubMed: 32254056]
131. Zhou Y, MacKinnon R. 2003. The occupancy of ions in the K^+ selectivity filter: charge balance and coupling of ion binding to a protein conformational change underlie high conduction rates. J. Mol. Biol 333:965–75 [PubMed: 14583193]
132. Köpfer DA, Song C, Gruene T, Sheldrick GM, Zachariae U, de Groot BL. 2014. Ion permeation in K^+ channels occurs by direct coulomb knock-on. Science 346:352–55 [PubMed: 25324389]
133. Chin D, Means AR. 2000. Calmodulin: a prototypical calcium sensor. Trends Cell Biol. 10:322–28 [PubMed: 10884684]
134. Denisov IG, Makris TM, Sligar SG, Schlichting I. 2005. Structure and chemistry of cytochrome P450. Chem. Rev 105:2253–78 [PubMed: 15941214]
135. Atkins WM, Sligar SG. 1989. Molecular recognition in cytochrome P-450: alteration of regioselective alkane hydroxylation via protein engineering. J. Am. Chem. Soc 111:2715–17
136. Lee Y-T, Wilson RF, Rupniewski I, Goodin DB. 2010. P450cam visits an open conformation in the absence of substrate. Biochemistry 49:3412–19 [PubMed: 20297780]
137. Fournier F, Guo R, Gardner EM, Donaldson PM, Loeffeld C, et al. 2009. Biological and biomedical applications of two-dimensional vibrational spectroscopy: proteomics, imaging, and structural analysis. Acc. Chem. Res 42:1322–31 [PubMed: 19548660]
138. Hume S, Hithell G, Greetham GM, Donaldson PM, Towrie M, et al. 2019. Measuring proteins in H_2O with 2D-IR spectroscopy. Chem. Sci 10:6448–56 [PubMed: 31341597]
139. Hume S, Greetham GM, Donaldson PM, Towrie M, Parker AW, et al. 2020. 2D-infrared spectroscopy of proteins in water: using the solvent thermal response as an internal standard. Anal. Chem 92:3463–69 [PubMed: 31985198]
140. Le Sueur AL, Ramos S, Ellefsen JD, Cook SP, Thielges MC. 2017. Evaluation of *p*-(^{13}C,^{15}N-cyano)phenylalanine as an extended timescale 2D IR probe of proteins. Anal. Chem 89:5254–60 [PubMed: 28406611]
141. Park K-H, Jeon J, Park Y, Lee S, Kwon H-J, et al. 2013. Infrared probes based on nitrile-derivatized prolines: thermal insulation effect and enhanced dynamic range. J. Phys. Chem. Lett 4:2105–10
142. Levin DE, Schmitz AJ, Hines SM, Hines KJ, Tucker MJ, et al. 2016. Synthesis and evaluation of the sensitivity and vibrational lifetimes of thiocyanate and selenocyanate infrared reporters. RSC Adv. 6:36231–37
143. Ramos S, Scott KJ, Horness RE, Le Sueur AL, Thielges MC. 2017. Extended timescale 2D IR probes of proteins: *p*-cyanoselenophenylalanine. Phys. Chem. Chem. Phys 19:10081–86 [PubMed: 28367555]
144. Chalyavi F, Schmitz AJ, Fetto NR, Tucker MJ, Brewer SH, Fenlon EE. 2020. Extending the vibrational lifetime of azides with heavy atoms. Phys. Chem. Chem. Phys 22:18007–13 [PubMed: 32749405]
145. Baiz CR, Kubarych KJ. 2011. Ultrabroadband detection of a mid-IR continuum by chirped-pulse up-conversion. Opt. Lett 36:187–89 [PubMed: 21263495]
146. De Marco L, Ramasesha K, Tokmakoff A. 2013. Experimental evidence of Fermi resonances in isotopically dilute water from ultrafast broadband IR spectroscopy. J. Phys. Chem. B 117:15319–27 [PubMed: 23638966]

147. Stingel AM, Calabrese C, Petersen PB. 2013. Strong intermolecular vibrational coupling through cyclic hydrogen-bonded structures revealed by ultrafast continuum mid-IR spectroscopy. J. Phys. Chem. B 117:15714–19 [PubMed: 24015677]

148. Singh V, Peng CS, Li D, Mitra K, Silvestre KJ, et al. 2014. Direct observation of multiple tautomers of oxythiamine and their recognition by the thiamine pyrophosphate riboswitch. ACS Chem. Biol 9:227–36 [PubMed: 24252063]

149. Bruening EM, Schauss J, Siebert T, Fingerhut BP, Elsaesser T. 2018. Vibrational dynamics and couplings of the hydrated RNA backbone: a two-dimensional infrared study. J. Phys. Chem. Lett 9:583–87 [PubMed: 29337564]

150. Sanstead PJ, Tokmakoff A. 2018. Direct observation of activated kinetics and downhill dynamics in DNA dehybridization. J. Phys. Chem. B 122:3088–100 [PubMed: 29504399]

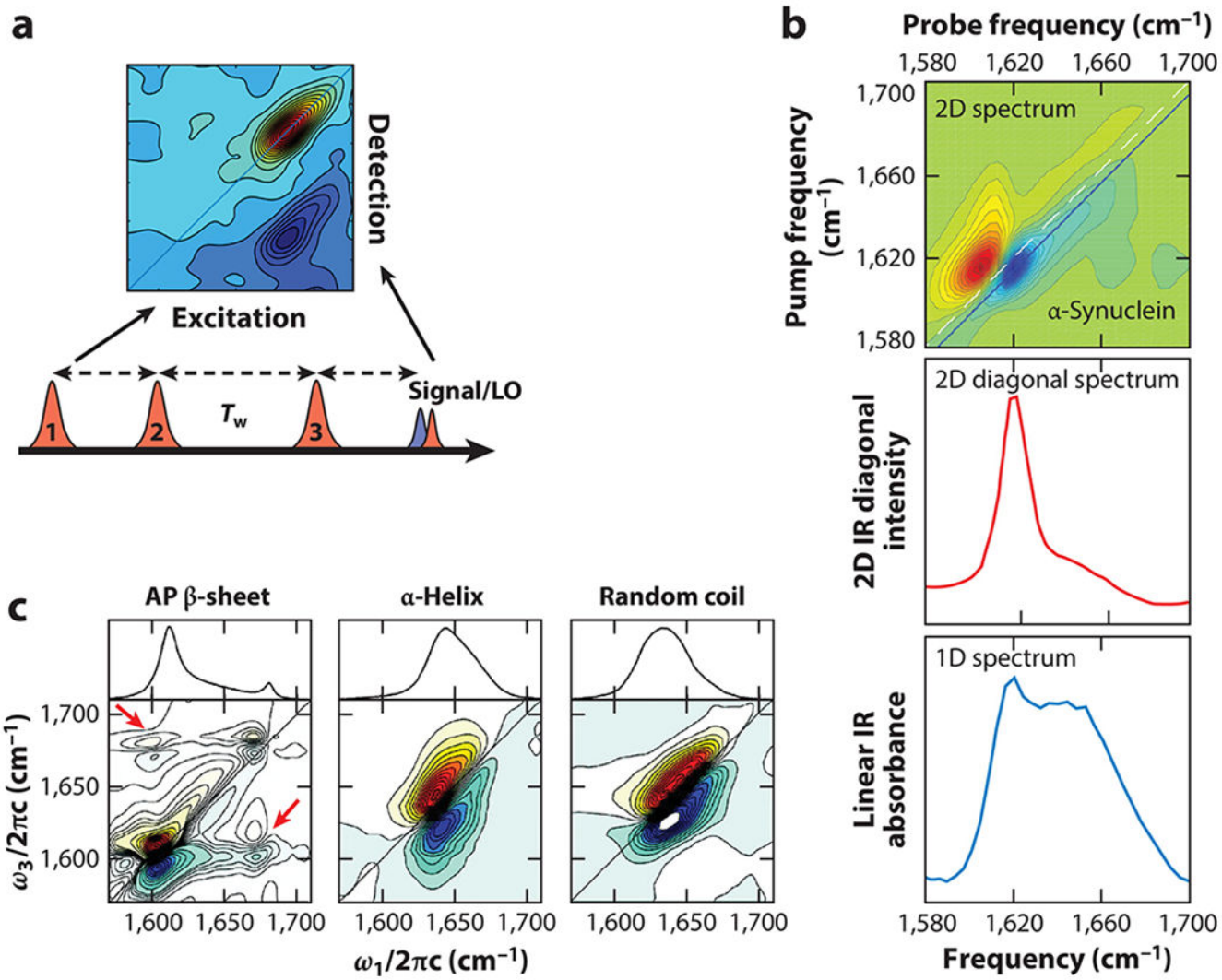

Figure 1.

(*a*) Example 2D spectrum of a single vibrational mode showing a pair of oppositely signed bands (*top*) and schematic of a three-pulse sequence of a 2D IR experiment (*bottom*). (*b*) 2D spectrum, 2D diagonal spectrum, and 1D spectrum for amide region of α-synuclein. Panel adapted with permission from Reference 29; copyright 2017 American Chemical Society. (*c*) Amide 2D spectra illustrating signatures of β-sheet, α-helix, and random coil secondary structure. Red arrows demark crossbands due to transition dipole coupling. Panel adapted with permission from Reference 4; copyright 2008 American Chemical Society. Abbreviations: 2D IR, two-dimensional infrared spectroscopy; AP, anti-parallel; LO, local oscillator; T_w, waiting time.

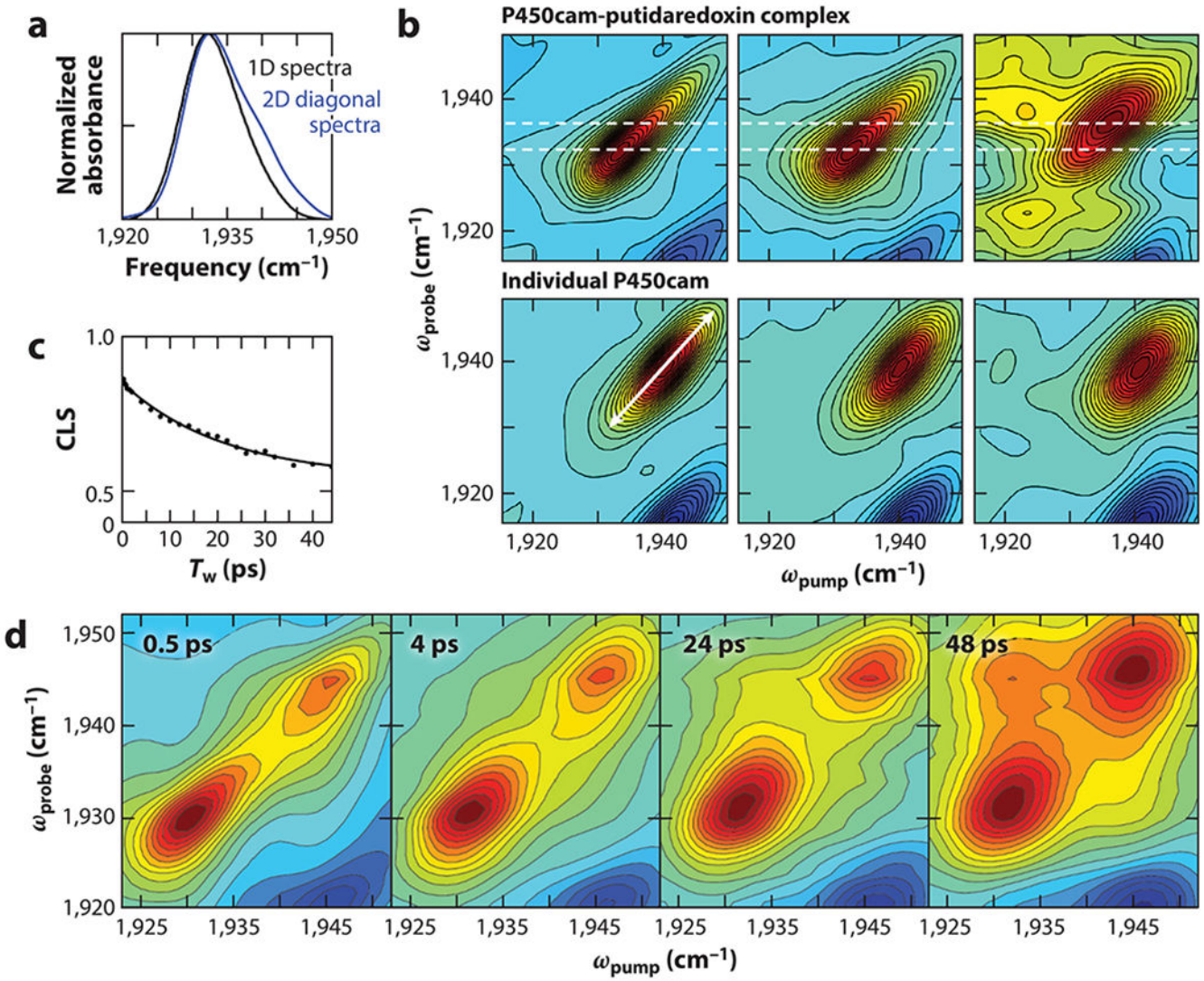

Figure 2.

(*a–c*) Spectral data for CO ligated to cytochrome P450cam and its complex with putidaredoxin. (*a*) Overlay of 1D and 2D diagonal spectra of P450cam-putidaredoxin complex normalized by maximum absorbance. (*b*) T_w-dependent 2D spectra of the P450cam-putidaredoxin complex and individual P450cam. The white dashed lines demark the center frequencies of the two component bands. The white arrow illustrates the diagonal elongation of the 2D band due to inhomogeneous broadening. (*c*) CLS decay from 2D lineshape analysis for individual P450cam. Panels *a–c* adapted from Reference 32. (*d*). T_w-dependent 2D spectra of CO ligated to myoglobin. Panel adapted with permission from Reference 36; copyright 2008 National Academy of Sciences. Abbreviations: CLS, center-line-slope; CO, carbon monoxide; T_w, waiting time.

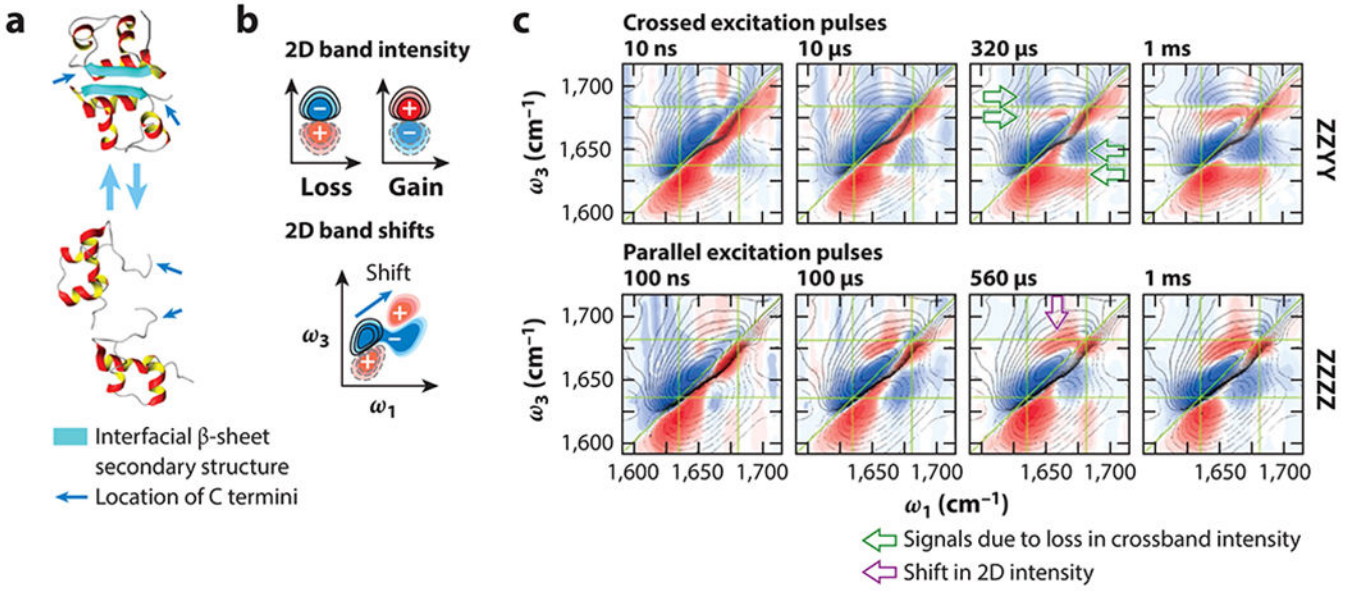

Figure 3.

(*a*) Illustration of insulin dimer dissociation and loss of interfacial β-sheet secondary structure (*aqua*). (*b*) Schematic of 2D patterns characteristic of gain or loss of 2D band intensity or of 2D band shifts. (*c*) Transient 2D difference spectra following rapid heating taken with crossed and parallel excitation pulses. Figure adapted with permission from Reference 63; copyright 2016 American Chemical Society.

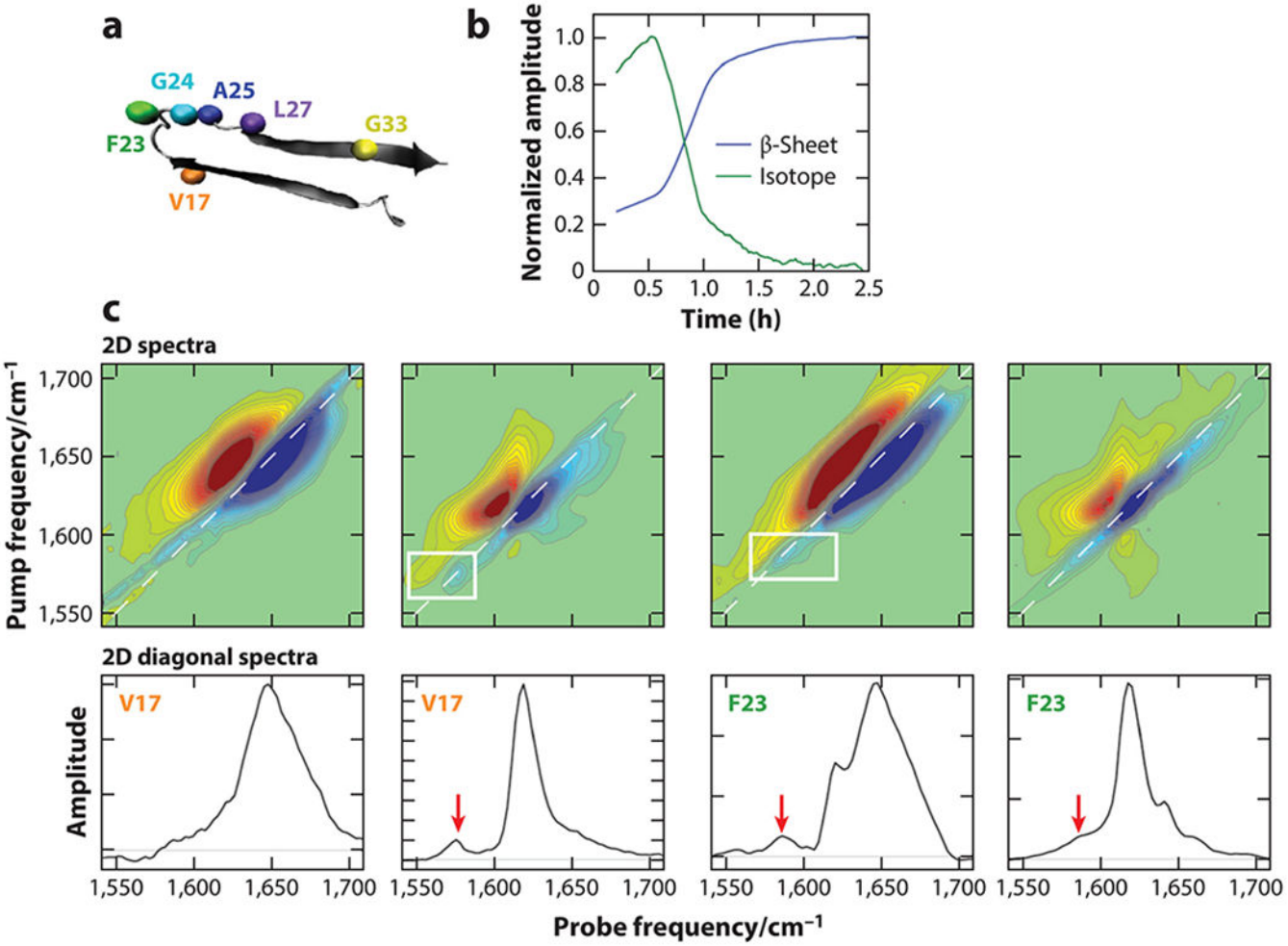

Figure 4.

(*a*) Ribbon depiction of β-sheet backbone structure of human islet polypeptide (hIAPP) fibrils; beads mark residues individually labeled with $^{13}C^{18}O$. (*b*) Kinetic traces following global sigmoidal transition of unlabeled β-sheet (1,620 cm^{-1}, *blue*) and growth of intermediate β-sheet absorbance for isotope-labeled mode (1,587 cm^{-1}, *green*) for F23. (*c*) 2D spectrum and 2D diagonal spectrum taken at an early time of lag phase (*left columns*) and late time of equilibrated phase (*right columns*) for $^{13}C^{18}O$ labeled at V17 and F23. Absorptions of isotope-labeled modes associated with β-sheet structure are highlighted with white boxes and red arrows. Figure adapted from Reference 61.

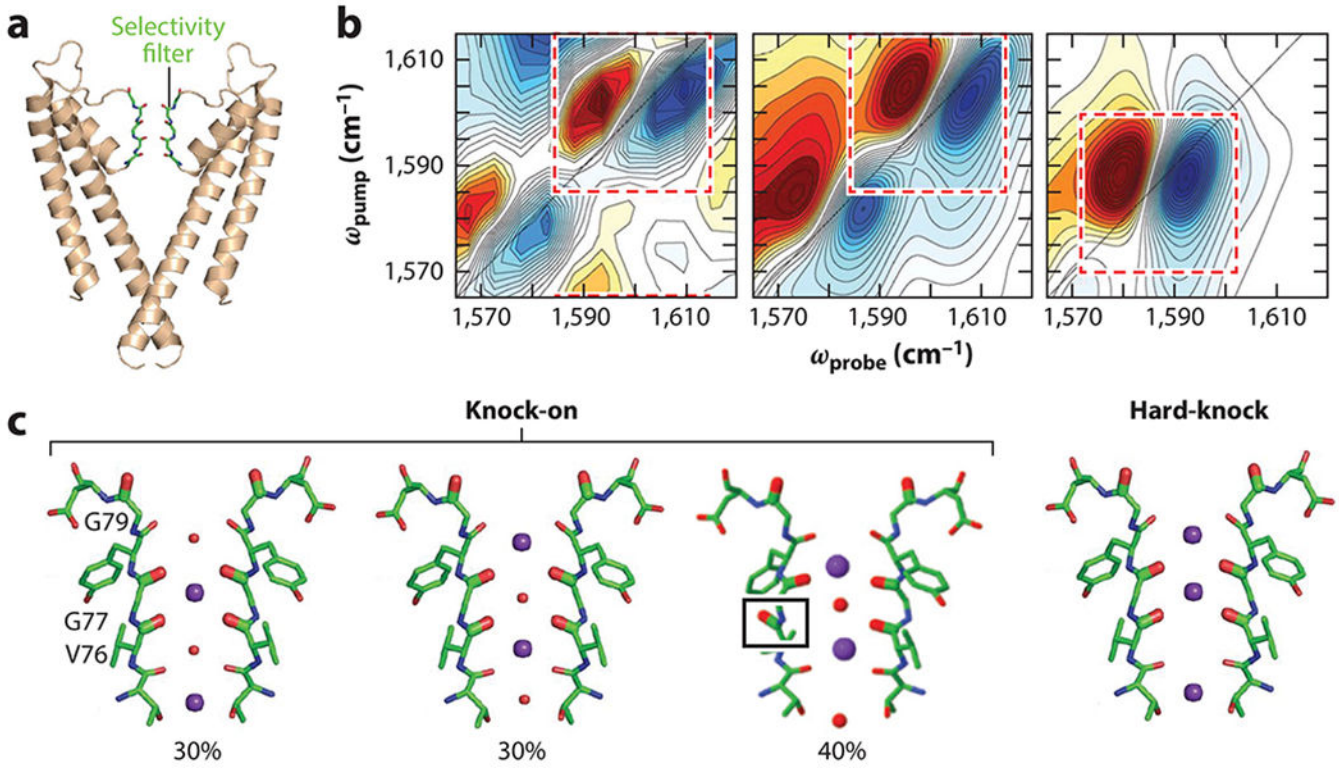

Figure 5.

(*a*) Ribbon structure of backbone of two subunits of the ion channel KcsA with the backbone of residues of the selectivity channel highlighted in green. (*b*) Experimental 2D spectrum of KcsA selectively labeled with $^{13}C^{18}O$ (*left*) and simulated 2D spectrum based on the knock-on (*middle*) and hard-knock (*right*) models. (*c*) Structures of configurations of the selectivity filter adopted for the knock-on (*left*) and hard-knock (*right*) models. A box highlights the flip in the backbone of V76. Figure adapted with permission from Reference 67; copyright 2016 AAAS.

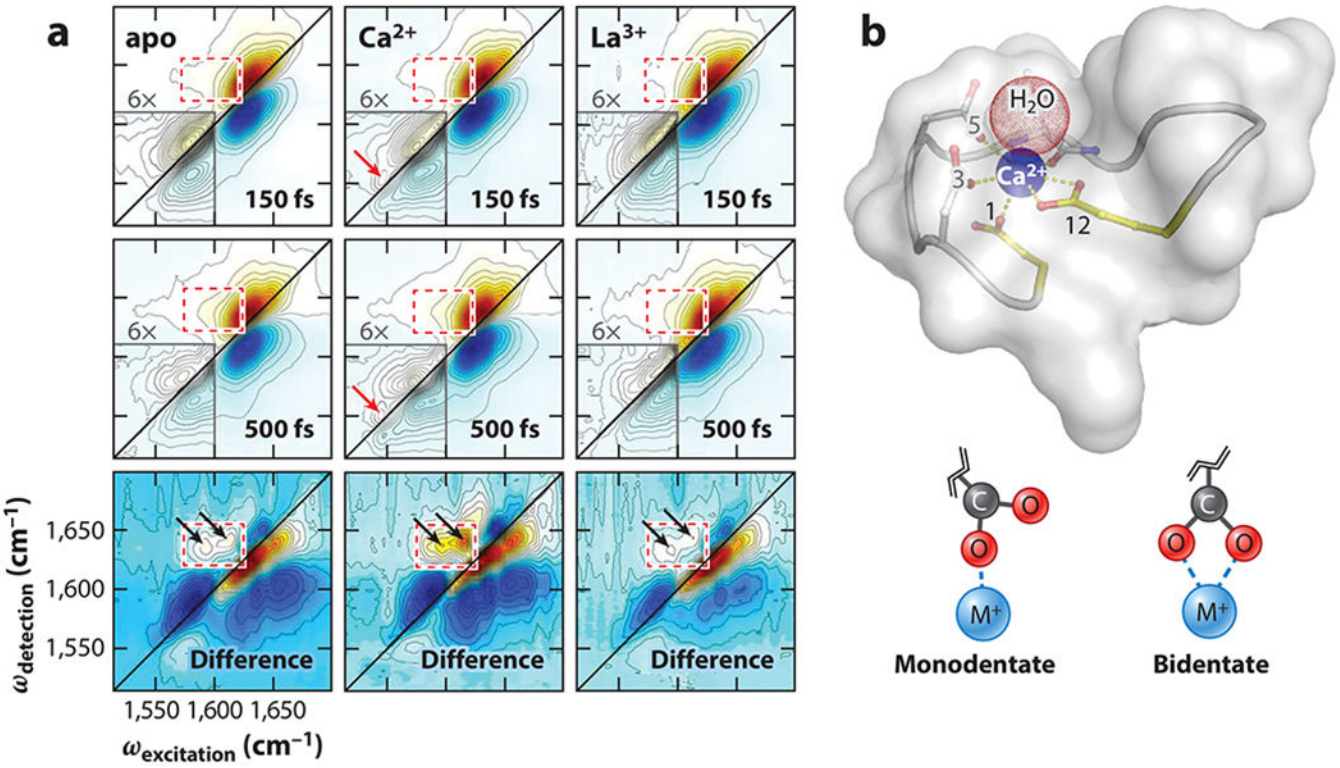

Figure 6.

(*a*) 2D spectra of apoprotein and Ca^{2+}-bound and La^{3+}-bound CaM taken with T_w of 150 fs, 500 fs, and their difference. The region of carboxylate absorptions is expanded 6×. The red arrows mark carboxyl absorptions associated with bidentate coordination; black arrows highlight crossbands. (*b*) Structural model of the Ca^{2+}-binding site of CaM, highlighting conserved residue Glu12 and other ion ligands (*top*) and schematic of ion coordination modes (*bottom*). Figure adapted from Reference 69. Abbreviations: CaM, calmodulin; T_w, waiting time.

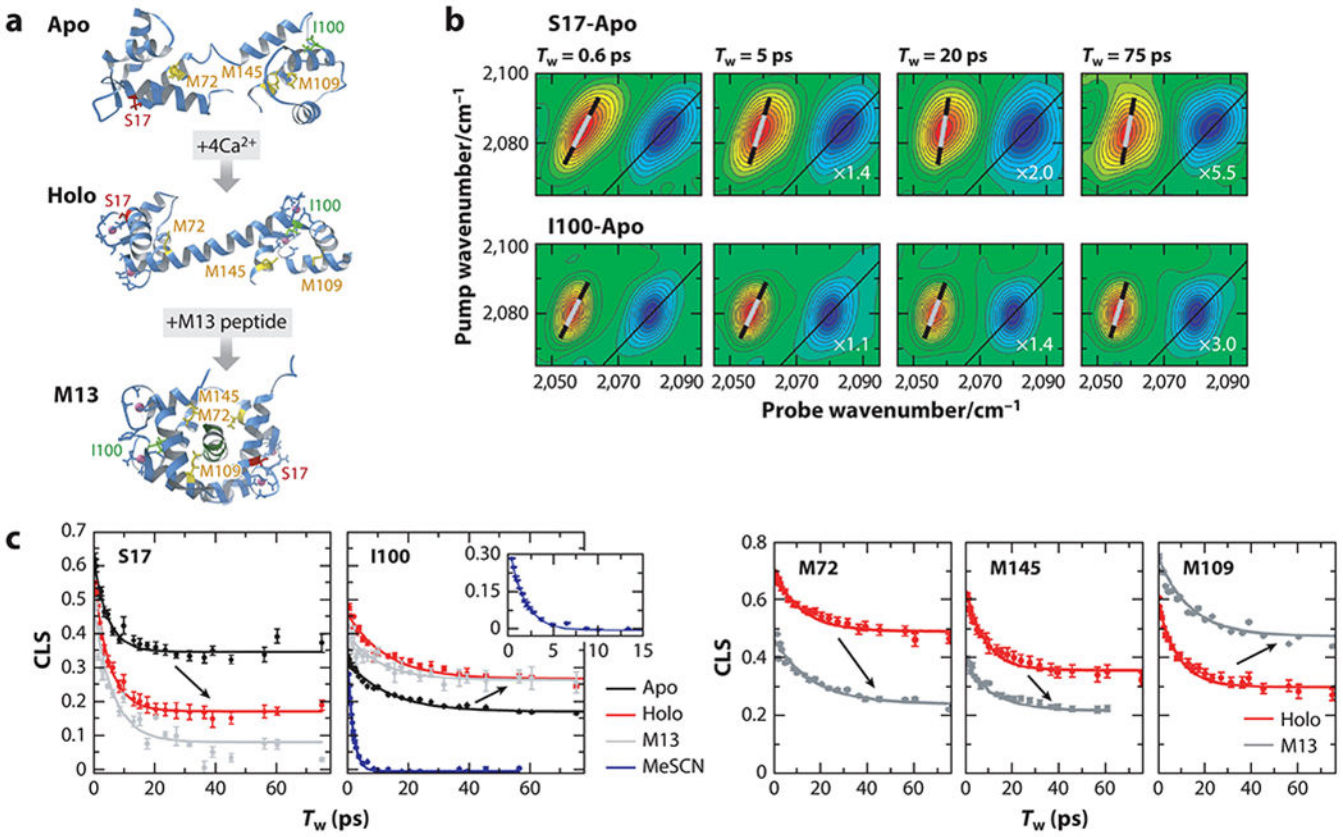

Figure 7.

(*a*) Ribbon structures of the backbone of CaM domain showing conformational changes induced by ion and peptide ligand binding. Side chains of residues of *CN*SCys incorporation are depicted as colored sticks and labeled. (*b*) Example T_w-dependent 2D spectra for *CN*SCys incorporated at residues S17 (*top*) and I100 (*bottom*) of apoprotein. Lines on each 2D spectrum depict the center line metric. (*c*) CLS decays for each *CN*SCys for the apoprotein (*black*) and after binding Ca^{2+} (*red*) and the peptide ligand (*gray*). Figure adapted with permission from Reference 92; copyright 2020 Physical Chemistry Chemical Physics. Abbreviations: CaM, calmodulin; CLS, center-line-slope; *CN*SCys, thiocyanocysteine; T_w, waiting time.

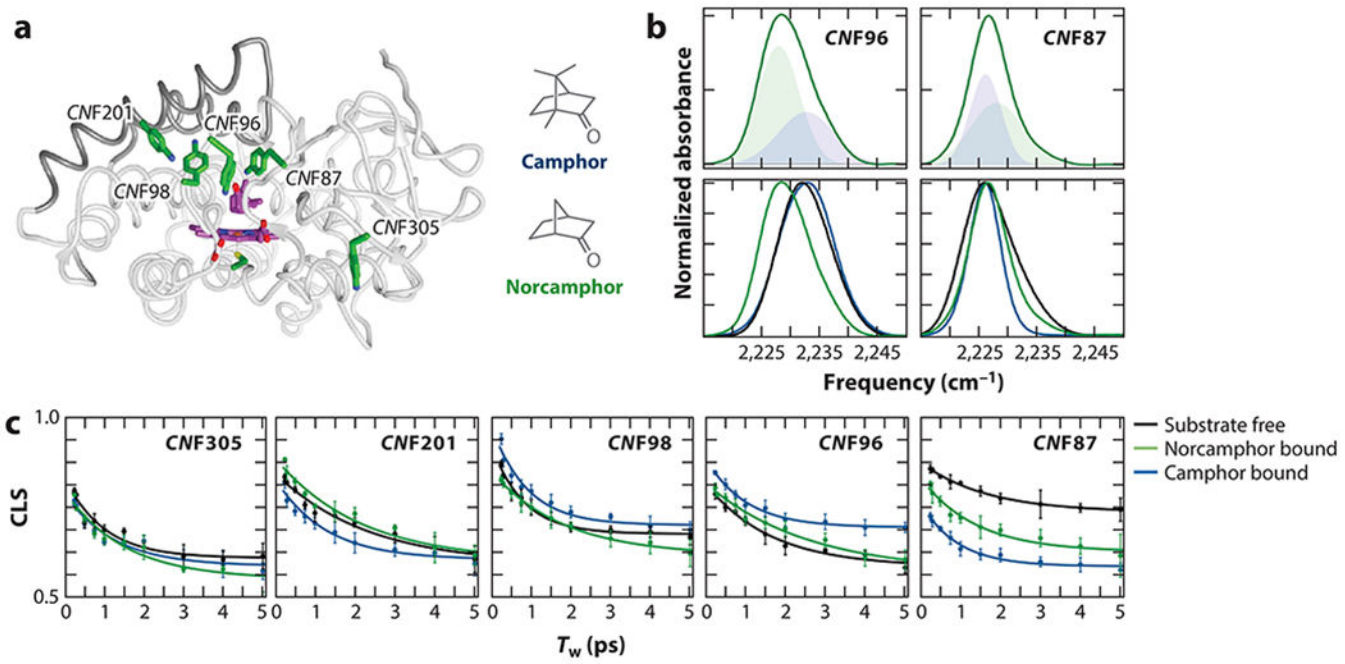

Figure 8.

(*a*) Ribbon structure of the backbone of P450cam with side chains of incorporated *CN*F shown in green, and the structures of camphor and norcamphor substrates. (*b*) 1D spectra of *CN*F96 (*left*) and *CN*F87 (*right*) P450cam for the norcamphor complex. Gaussian component bands are shaded (*top row*), and the spectra for substrate free (*black*), camphor complex (*blue*), and norcamphor complex (*green*) are overlaid (*bottom row*). (*c*) CLS decays for each *CN*F probe for substrate free (*black*), norcamphor complex (*green*), and camphor complex (*blue*). Figure adapted with permission from Reference 93; copyright 2021 Elsevier. Abbreviations: CLS, center-line-slope; *CN*F, cyanophenylalanine.